Mismatched Heteroepitaxy of Tetrahedral Semiconductors with Si via ZrB_2 Templates

Rahul Trivedi,[†] Po−Liang Liu,[‡] Radek Roucka,[†] John Tolle,[†] Andrew V. G. Chizmeshya,[§] Ignatius S. T. Tsong,[‡] and John Kouvetakis*,[†]

Department of Chemistry and Biochemistry, Department of Physics and Astronomy, and Center for Solid State Science, Arizona State University, Tempe, Arizona 85287

Received May 21, 2005. Revised Manuscript Received June 21, 2005

We demonstrate integration of cubic SiC (heterostructures and nanostructures) and assemblies of Ge nanoscale islands with Si substrates via a conductive and reflective ZrB_2 buffer layer. Hexagonal ZrB_2 is grown on cubic Si(111) via a coincidence-misfit mechanism in which the strain is accommodated by edge dislocations along the interface. Ge islands with uniform sizes and strain-free microstructures were grown on ZrB_2/Si(111) at 500 °C via thermolysis of Ge_2H_6, circumventing the strain-driven (Stranski−Krastanov) island formation on Si and associated limitations. Heteroepitaxy between ZrB_2(0001) and Ge(111) is obtained via alignment of four lattice rows of Ge with every five rows of ZrB_2, (i.e., "magic mismatch") despite the large difference in lattice constants. Cubic SiC layers with monocrystalline microstructures and atomically abrupt interfaces are grown on ZrB_2/Si(111) via single source molecular beam epitaxy of $C_2(SiH_3)_2$ at 800 °C. Nanoscale SiC islands with perfectly coherent zinc blende structures are formed at higher temperatures such as 900 °C. The SiC(111)/ZrB_2 interface structures were examined in both cases with high-resolution electron microscopy and compared with optimal bonding configurations derived from theoretical models.

Introduction

The classic heteroepitaxy concept is based on integration of materials with closely matched crystal structures, lattice dimensions, and thermoelastic properties (thermal expansion coefficients and stiffness). Integrations of dissimilar, lattice-mismatched systems (both relaxed and strained) have been of general interest but in many cases difficult to achieve as a result of lack of suitable templates.[1−3] The realization of this capability, especially on Si substrates, could significantly enhance device performance and reduce the production cost for many electronic and optoelectronics systems. Accordingly, heteroepitaxial growth studies are currently being pursued to identify suitable template architectures that would promote integration of fully relaxed films and allow engineering of their defect structures (e.g., introducing appropriate misfit dislocation arrays and minimizing threading dislocations). Recently we have demonstrated epitaxial growth of superhard, metallic ZrB_2 films directly on Si(111) despite the ∼20% mismatch between the two materials [the Si−Si in-plane distance in Si(111) is 3.84 Å and the ZrB_2 parameter "*a*" of the hexagonal structure is 3.17 Å].[4] The ZrB_2 layers are used as templates for subsequent growth of structurally dissimilar AlGaN and GaN epitaxial layers with superior luminescent and structural properties.[5,6] The ZrB_2 film serves as a reflecting intermediate layer, which prevents any loss of emission intensity from the light-emitting GaN and AlGaN overlayers into the absorbing Si substrate.

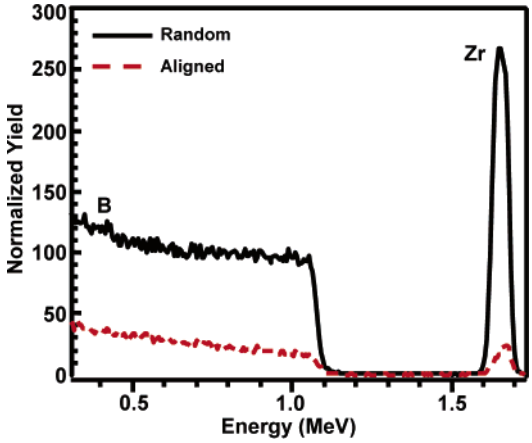

Figure 1. RBS random and channeled spectra of a 30 nm ZrB_2 film grown on Si(111). The high degree of channeling in the film indicates well-aligned material.

Our ZrB_2 films are directly grown on a clean Si(111) surface via a single source epitaxy of $Zr(BH_4)_4$ at 900 °C.[4−5] X-ray diffraction (XRD) and atomic force microscopy (AFM) indicate highly aligned monocrystalline structures with atomically planar surfaces. Rutherford backscattering (RBS) ion channeling confirms commensurate growth of hexagonal ZrB_2 on cubic Si(111). Figure 1 compares the RBS random

* Corresponding author. E-mail: jkouvetakis@asu.edu.
[†] Department of Chemistry and Biochemistry.
[‡] Department of Physics and Astronomy.
[§] Center for Solid State Science.

(1) Golding, T. D.; Holland, O. W.; Kim, M. J.; Dinan, J. H.; Almeida, L. A.; Arias, J. M.; Bajaj, J.; Shih, H. D.; Kirk, W. P. *J. Electron. Mater.* **2003**, *32*, 882.
(2) Sarney, W. L.; Brill, G. *Solid State Electronics* **2004**, *48*, 1917.
(3) Lee, M. L.; Pitera, A. J.; Fitzgerald, E. A. *J. Vac. Sci. Technol. B* **2004**, *22*, 158.
(4) Hu, C.-W.; Chizmeshya, A. V. G.; Tolle, J.; Kouvetakis, J.; Tsong, I. S. T. *J. Cryst. Growth* **2004**, *267* (3−4), 554.
(5) Tolle, J.; Roucka, R.; Tsong, I. S. T.; Ritter, C.; Crozier, P. A.; Chizmeshya, A. V. G.; Kouvetakis, J. *J. Appl. Phys.* **2003**, *82* (15), 2398.
(6) Tolle, J.; Kim, D.; Mahajan, S.; Bell, A.; Ponce, F. A.; Kottke, M.; Kouvetakis J.; Tsong, I. S. T. *Appl. Phys. Lett.* **2004**, *84*, 3510.

10.1021/cm0510918 CCC: $30.25
Published on Web 08/12/2005

and channeled spectra along ZrB_2(0001)/Si(111). The ratio of the aligned versus the random peak heights (χ_{min}), which measures the degree of crystallinity and heteroepitaxial alignment across the layer, is ~6%. This value approaches the practical limit of ~3% for a defect-free Si crystal. The epitaxial registry between the Si(111) and ZrB_2 has been characterized extensively by high-resolution electron microscopy (cross-sectional transmission electron microscopy, XTEM) including Z-contrast imaging of the interface. The results show that the misfit is taken up by pure edge-type dislocations from the insertion of extra $\{1\bar{1}00\}$ lattice planes along the $[11\bar{2}0]$ direction.[4,5] No threading dislocation cores propagate in the direction normal to the substrate. The exceptional epitaxial alignment between Si(111) and ZrB_2 and its subsequent use for integration of Al−Ga−N based materials[6] with Si prompted us to explore growth of related Si-based materials such as elemental Ge and cubic SiC on ZrB_2 buffer layers. The objective is to form strain-free, epitaxial materials and investigate their optical and thermoelastic properties.

In the case of Ge, the high surface energy with respect to ZrB_2 is likely to promote formation of islands rather than continuous planar films. This is particularly attractive and would allow us to explore growth of Ge quantum dots with coherent and completely strain-free microstructures and uniform size distributions. This concept will circumvent difficulties typically encountered in the direct growth of Ge quantum dots on Si via the Stranski−Krastanov mechanism.[7] The successful growth of Ge quantum dots with high structural and morphological quality on reflecting surfaces may have applications in IR laser technologies and related high-efficiency optoelectronic devices.

Silicon carbide is another material of interest due to its unique thermal and electronic properties. The availability of a thermal oxide makes SiC a suitable candidate for high-power, high-speed, high-temperature, and radiation-resistant applications.[8] One of the most interesting properties of SiC is the occurrence of structural polytypes (due to a relatively small difference in their energies), with different properties.[9] Of particular technological interest is the β-SiC cubic phase, which has a relatively narrow band gap of 2.2 eV and displays important properties such as a high junction breakdown electric field and high thermal conductivity. β-SiC also possesses a high saturated electron drift velocity due to reduced phonon scattering, compared to its other polytypes.[10] Efforts to grow hetero-epitaxial β-SiC on Si substrates have met with limited success as a result of a large (~20%) lattice mismatch and a thermal expansion mismatch.[11] Significant work has concentrated on the use of novel precursors for the growth of β-SiC, which would enable control of stoichiometry and favor low growth temperatures.[12−14] In this paper, we report growth of β-SiC heterostructures and nanostructures on silicon(111) via a zirconium diboride template, which provides a practical route to integration with silicon.

Growth of Ge on ZrB_2

The current methods for synthesis of nanoscale Ge islands involve almost exclusively molecular beam epitaxy (MBE) growth on Si(100) substrates.[15] Self-assembled structures form readily on the Si surface after initial growth of a wetting layer (three monolayers thick) as a means of relieving the inherent compressive strain between the larger Ge and the smaller Si lattice.[15] Initially the islands are coherent square pyramids that eventually transform into domed shaped structures with increasing size and volume.[16] As the domes become even larger they show a tendency to relieve strain via formation of misfit dislocations and threading defects, which are detrimental to the optical and electronic properties of the material. It has been found that at temperatures above 550 °C silicon from the underlying substrate diffuses into the Ge islands to form alloys with graded compositions and blurred nonuniform interfaces.[17] Alternate approaches involving epitaxial growth on virtual substrates and buffer layers that can accommodate the lattice and thermal mismatch are, therefore, of interest. The main objective is to circumvent entirely strain-driven island formation and the associated problems. These include reaction with the substrate at moderate temperatures, size variations, broad distribution of residual strain among dots leading to nonuniformities of the electronic structure, the presence of strained wetting layers, and most importantly the development of dislocations due to the lattice mismatch. In the ZrB_2(0001)/Ge(111) system the in-plane lattice mismatch between Ge and ZrB_2 is very large (~20% between $d_{Ge-Ge} = 3.995$ Å and $a_{ZrB_2} = 3.189$ Å). Nevertheless, the ratio of the parameters d_{Ge-Ge}/a_{ZrB_2} gives 1.252, which translates into a nearly perfect coincidence of five ZrB_2 lattice planes with four Ge lattice planes (5/4 = 1.25), which may promote heteroepitaxial growth. A similar mismatch of 4:5 between cubic GaN and GaAs(001) has been reported previously for the epitaxial growth of lattice-mismatched GaN on GaAs(001).[18] In addition the bulk modulus of ZrB_2 (260 GPa) is much larger than that of Ge (76 GPa), which is similar to Si (90 GPa). This suggests that the Ge films should exhibit higher ductility (i.e., they are softer solids) than ZrB_2. In this regard the softer lattice of Ge may show the ability to relieve stress when grown on the "stiffer" ZrB_2 template via introduction of misfit edge dislocations in much the same way as the

(7) Ross, F. M.; Tromp, R. M.; Reuter, M. C. *Science* **1999**, *286*, 1931.
(8) Davis, R. F. Kelner, G.; Shur, M.; Palmour, J. W.; Edmond, J. A. *Proc. IEEE* **1991**, 677.
(9) Bechstdet, F.; Kackell, P.; Zywietz, A.; Karch, K.; Adolph, B.; Tenelsen, K.; Furthmuller, J. *Silicon Carbide: A Review of Fundamental Questions and Applications to Current Device Technology*; John Wiley and Sons Inc.: Switzerland, 1997; p 5.
(10) Das, P.; Ferry, D. K. *Solid-State Electron.* **1976**, *19*, 851.
(11) Nutt, S. R.; Smith, D. J.; Kim, H. J.; Davis, R. F. *Appl. Phys. Lett.* **1987**, *50* (4), 203.
(12) Wu, C. H.; Jacob, C.; Ning, X. J.; Nishino, S.; Pirouz, P. *J. Cryst. Growth* **1996**, *158* (4), 480.
(13) Boo, J. H.; Yu, K. S.; Lee, M.; Kim, Y. *Appl. Phys. Lett.* **1995**, *66* (25), 3486.
(14) Chaddha, A. K.; Parsons, J. D.; Wu, J.; Chen, H.-S.; Roberts, D. A.; Hockenhull, H. *Appl. Phys. Lett.* **1993**, *62*, 3097.
(15) Tromp, R. M.; Ross, F. M.; Reuter, M. C. *Phys. Rev. Lett.* **2000**, *84*, 461.
(16) Medeiros-Rebeiro, G.; Bratkovski, A.; Kamins. T.; Ohlberg, D.; Williams R. *Science* **1998**, *279*, 353.
(17) Chaparo, S.; Zhang, Y.; Drucker, J.; Chandasekhar, D.; McCartney, M.; Smith, D. *J. Phys. Rev. Lett.* **2000**, *87*, 2245.
(18) Trampert, A.; Brandt, O.; Yang, H.; Ploog, K. H. *Appl. Phys. Lett.* **1997**, *70*, 583.

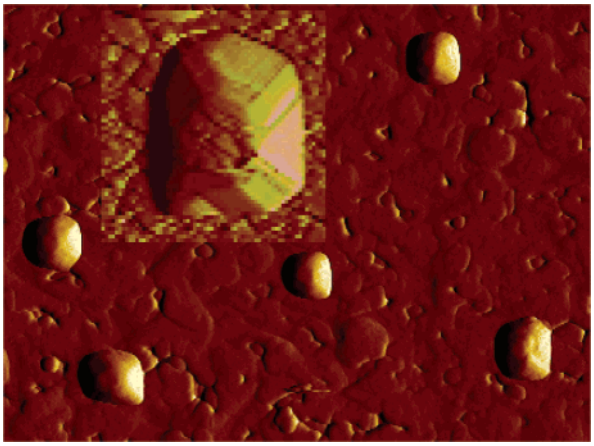

Figure 2. AFM image of Ge dome-shaped islands grown on a flat ZrB_2 buffer layer. The inset is an enlarged view of a typical faceted island.

Si(111)/ZrB_2 system accommodates its differential stress because of the large mismatch at the interface. Formation of edge dislocations that are localized along the heterojunction is more desirable than threading defects that propagate through the film and cause degradation of key film properties.

The ZrB_2 films were grown and characterized ex situ in all cases to assess their morphological and structural quality for use as potential templates. Only films that displayed a root-mean-square (RMS) roughness of ~1 nm, RBS x_{min} channeling of ~5−7%, and XRD (0001) rocking curves with a full width at half-maximum (fwhm) of less than 0.07° were utilized for subsequent growth. The characterized templates were cleaned in acetone, 2-propanol, and methanol ultrasonic baths prior to use. They were then loaded in the growth chamber via a load lock and outgassed overnight at 800 °C until the pressure inside the growth chamber reached the base value of 2×10^{-10} Torr. Heating was achieved by passing a current through the sample, and the temperature was measured using an optical pyrometer. The growth was conducted at 550−600 °C via decomposition reactions of pure digermane. The gaseous precursor was admitted into the chamber via a nozzle located 1−2 in. away from the substrate surface, and its flow was controlled by adjusting a needle valve. The optimum deposition pressure inside the chamber was in the range of 10^{-7} Torr. The typical duration of sample growth was 30−60 min.

The samples were characterized by XRD, AFM, RBS, and high-resolution transmission electron microscopy (HRTEM). A representative result of our deposition studies is illustrated by the AFM images in Figure 2. The data were obtained from a sample of pure Ge grown on ZrB_2 via deposition of digermane (Ge_2H_6) at 500 °C. The AFM scans show assemblies of faceted Ge nanoscale islands grown on a smooth and continuous ZrB_2 surface. The AFM RMS roughness between islands is ~1 nm. The islands are primarily dome shaped with a width of ~45−50 nm at the base and a height of 15−20 nm. The domes exhibit {105}, {113}, {15 3 23}, or even steeper facets that are essentially identical to those observed in pure Ge islands with similar shapes and sizes grown directly on Si. The X-ray patterns showed the characteristic (111) reflection of the cubic structure with a *d* spacing identical to that of bulk Ge, indicating that the material is fully relaxed. The bright-field

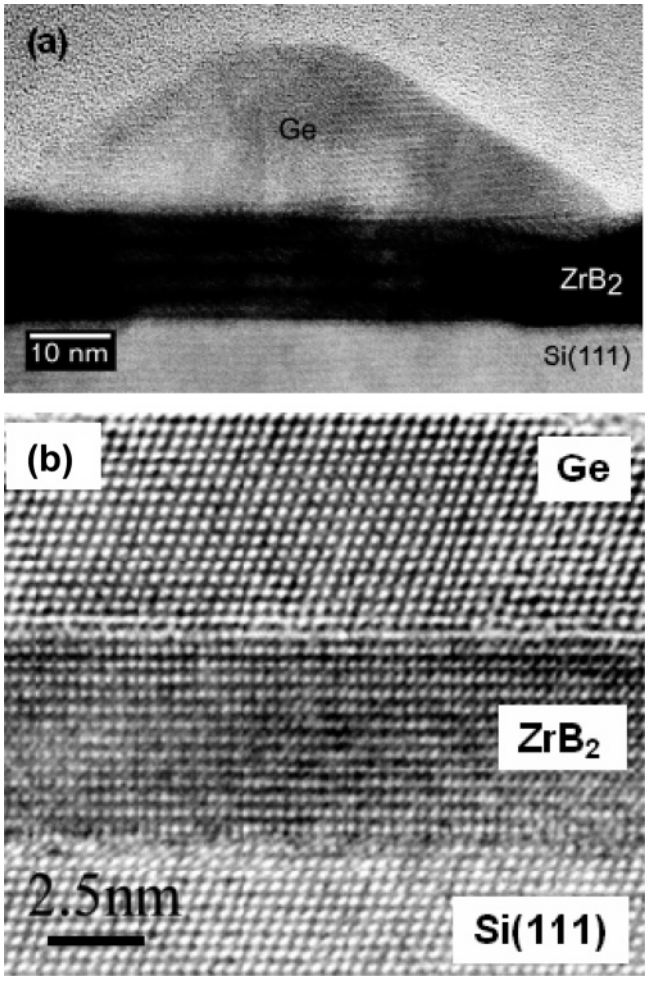

Figure 3. (top) Bright-field XTEM image showing the typical shape, size, and microstructure of a Ge island on ZrB_2. (bottom) High-resolution image of the entire Si(111)/ZrB_2(0001)/Ge(111) heterostructure showing perfect epitaxial alignment between the layers and the substrate.

XTEM images revealed uniform assemblies of highly coherent domes free of threading defects and a narrow size distribution. The bright-field image in Figure 3a represents the most commonly observed Ge island morphology, size, and microstructure. The corresponding high-resolution micrograph in Figure 3b shows a cross-sectional view of the Si(111)/ZrB_2(0001)/Ge(111) stack including the entire ZrB_2 layer thickness and its interfaces with Si and Ge. Note that the ZrB_2/Ge boundary is atomically sharp and shows an abrupt transition from the cubic Si(111) to the hexagonal ZrB_2(0001) lattice. While Si(111) has 3-fold symmetry, ZrB_2(0001) has 6-fold symmetry. The arrangement of the atomic columns perpendicular to the image in Figure 3b suggests that the Ge(111) is viewed along the $[\bar{1}10]$ direction and the ZrB_2(0001) is viewed along the $[11\bar{2}0]$ direction, that is, the growth axis is along [111] or [0001]. This leads to a heteroepitaxial relationship involving a coincidence mismatch of five ZrB_2 $\{1\bar{1}00\}$ lattice planes with four Ge$\{11\bar{2}\}$ lattice planes as discussed above. The high-resolution image of the ZrB_2/Ge interface in Figure 3b reveals that the misfit is taken up by pure edge-type dislocation from the insertion of extra $\{\bar{1}10\}$ lattice planes along the $[11\bar{2}0]$ direction in ZrB_2. No threading dislocation cores propagating in a direction normal to the substrate are observed in the bright-field TEM images. The high-resolution XTEM image

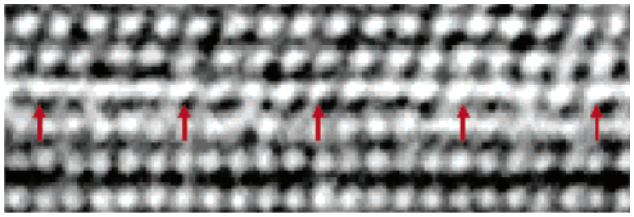

Figure 4. High-resolution XTEM image showing the 4:5 coincidence mismatch between Ge [$\bar{1}10$] and ZrB_2 [$11\bar{2}0$].

of the interface in Figure 4 shows exactly such a 5:4 coincidence. The arrows at the interface mark the commensuration length of ~16 Å comprising five ZrB_2 lattice rows to four Ge lattice rows. The occurrence of such an exact mismatch between hexagonal ZrB_2 and Ge(111) accounts for the epitaxial growth of Ge. It is interesting to note that the high-resolution image in Figure 3 shows an exact coincidence of 27 (111) lattice planes of Si to 26 (111) lattice planes of Ge. The 27/26 ratio equals 1.0385 and virtually matches the ratio of the lattice parameters $a_{Ge}/a_{Si} = 5.65/5.43 = 1.0390$ as expected for fully relaxed Ge films.

Growth of Epitaxial β-SiC

The SiC growth on ZrB_2 is achieved by gas source MBE of the unimolecular precursor disilylacetylene, $C_2(SiH_3)_2$. The lack of strong C−H bonds in this compound leads to a relatively low growth temperature in the 750−850 °C range. The molecular architecture of the precursor incorporates the C and Si atoms in the required stoichiometric ratio ensuring precise compositional control in the film. Optimum growth of SiC layers was achieved at 800−850 °C at a pressure of 1×10^{-6} Torr. Under these conditions, SiC films 15 nm thick and devoid of any stacking faults are obtained after a typical deposition time of 30 min. This gives a growth rate of ~0.5 nm/min. XRD analysis indicated that the films are aligned with the ZrB2(0001)/Si(111). The fwhm of the (111) rocking curves is 0.5°, which is normal for such highly mismatched systems and indicates tightly aligned crystal mosaics. The RMS roughness over a scan area of 25×25 μm^2 is ~2 nm, indicating a fairly planar surface. The AFM images showed flat top rod-shaped features oriented at an angle of 60° to each other. A pattern with similar features has been observed in the AFM images of crystalline ZrB_2 templates grown on Si(111). This implies preferential growth along low-energy directions common both in SiC and ZrB_2. The microstructure of the ZrB_2(0001)/Si(111) samples grown at 800 °C was studied by XTEM. High-resolution phase-contrast bright-field micrographs (not shown) reveal uniform layers with smooth surfaces devoid of stacking dislocations and threading defects within the field of view of the XTEM images. The upper limit based on the dimensions of the films visible by TEM is $10^7/cm^2$. TEM images of the interface region illustrate an atomically abrupt boundary between the SiC film and the underlying template (Figure 5). Note that bulklike (111) SiC planes are observed after only one monolayer of growth above the interface, consistent with zinc blende type microstructure in the epilayer.

Decompositions of the precursor in the range of 850−950 °C produced monocrystalline, oriented and epitaxial

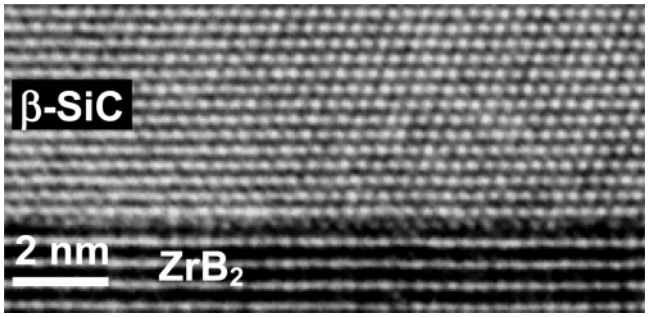

Figure 5. High-resolution image of β-SiC on ZrB_2. The transition between the hexagonal structure of the buffer layer and the cubic structure of the top layer occurs within a single plane growth.

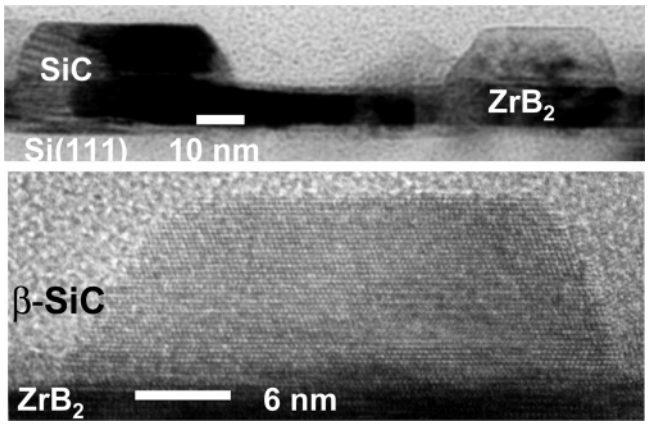

Figure 6. (top) Bright-field XTEM image showing the typical shape and size of SiC islands on ZrB_2. (bottom) High-resolution image showing the high-quality heteroepitaxy and cubic microstructure of a SiC island.

layers at significantly higher growth rates. These materials contained copious defects due to the enhanced decomposition of the precursor resulting in higher nucleation rates of the film. The high-resolution TEM images (not shown) revealed the presence of double positioning boundaries as a result of multiple nucleations and stacking faults. The TEM and XRD data revealed zinc blende type (cubic) structure, and the Fourier transform infrared and RBS spectra indicated stoichiometric SiC. To explore the formation of defect-free SiC films on ZrB_2 at higher temperatures, we also conducted growth via decomposition of SiH_3CH_3. In this case the compound decomposed on the template surface at 900 °C to produce assemblies of nanoscale islands rather than continuous films, as shown by the XTEM micrograph in Figure 6. These features grow epitaxially on the ZrB_2 surface and appear to be highly coherent. The typical island size is 25−30 nm wide at the base and 15 nm high. The film microstructure and the corresponding electron diffraction patterns are consistent with cubic SiC lattice. The lattice constants (determined by TEM and XRD) are virtually identical to those of bulk zinc blende SiC indicating formation of fully relaxed nanostructures. It should be noted that continuous films were not observed to form using a wide range of conditions via this synthesis route.

ZrB_2/β-SiC Interface Thermochemistry and Structure

The high-quality epitaxial formation of cubic SiC on hexagonal ZrB_2 takes place in spite the significant mismatch in the in-plane distances in SiC(111) (3.08 Å) and the corresponding lattice parameter a of ZrB_2 (3.17 Å). To

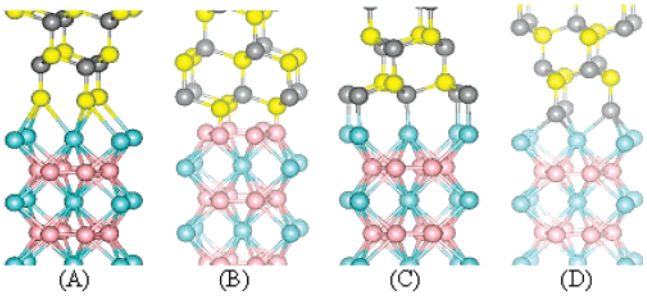

Figure 7. Models of the ZrB_2[0001] and SiC[111] interface structure showing the most favorable bonding arrangements derived from the ab initio studies. Yellow, black, blue, and pink spheres represent the atoms Si, C, Zr, and B, respectively.

expand our insight into the unusual epitaxial registry of this system we performed ab initio calculations to elucidate the crystallographic and thermodynamic properties of the interface structure. One objective is to identify the most stable bonding configuration that enables strain relaxation to be confined within a single boundary plane between the dissimilar materials. We studied the interface energy Γ of the SiC[111]−ZrB_2[0001] system in detail using standard GGA-based density functional theory.[19] The converged total slab energy of isolated ZrB_2 to SiC slabs was used to approximate[20] Γ, which is a general function of the chemical potentials of the constituents μ_{Zr}, μ_B, μ_{Si}, and μ_C. The thermodynamic equilibrium conditions $\mu_{Zr} + 2\mu_B = \mu_{ZrB_2}{}^{bulk}$ and $\mu_{Si} + \mu_C = \mu_{SiC}{}^{bulk}$ were used to reduce the interface energy to a function of only two parameters, namely, $\Gamma(\mu_C, \mu_{Zr})$. Bulk phase total energies were used to estimate the formation enthalpies yielding $\Delta H^f[ZrB_2] = -2.952$ eV and $\Delta H^f[SiC] = -0.54$ eV. These values are very close to those obtained in other density functional theory studies: $\Delta H^f[ZrB_2] = -3.076$ eV[21] and $\Delta H^f[SiC] = -0.58$ eV.[22] We obtain the bulk energy in terms of the energy difference, $E_{bulk}{}^{\alpha}$ ($E_{bulk}{}^{\beta}$), between two repeated slab geometries with 11 and 5 material α (β) layers separated by a vacuum region following the work of Boettger[23] The interface chemical potential of C spans a range from that in diamond (which we take as zero) to that of carbon in SiC (−0.54 eV). Similarly the calculation of bulk Zr and ZrB_2 yields $0 < \mu_{Zr} < -2.952$. The thermodynamic stability of various interface models was then studied by comparing their respective interface energies, $\Gamma_m(\mu_C, \mu_{Zr})$, over the allowed chemical potential range. A total of nine initial interface structure models, with specific bonding arrangements between ZrB_2(0001) and SiC(111) (with $ZrB_2[11\bar{2}0] \parallel SiC[1\bar{1}0]$), were constructed from known bulk geometries. Specifically, the interfaces include two types of Zr−Si, Zr−C, and B−C bonding arrangements, and three types of B−Si arrangements were considered. In Figure 7 we show the four most energetically favorable interfaces

Table 1. Interface Energies of the Four Models at the Four Limiting Values of the Allowed Silicon and Zirconium Chemical Potentials, Showing that Model A is Preferred[a]

model		Γ_A	Γ_B	Γ_C	Γ_D
C-rich	B-rich	0.1858	0.0453	0.2183	0.2878
C-rich	Zr-rich	0.0161	0.2150	0.0486	0.1181
Si-rich	B-rich	0.1547	0.0142	0.2494	0.3189
Si-rich	Zr-rich	−0.0150	0.1839	0.0797	0.1492

[a] Chemical potentials and interface energies are given in eV and eV/Å^2, respectively.

containing Zr−Si, B−Si, and Zr−C bonds. Because of the 3.2% mismatch in the basal dimensions of SiC (3.08 Å) and ZrB_2 (3.17 Å) we dilated the SiC lattice along the interface plane to match that of ZrB_2 (e.g., "coherent lattice approximation"). To allow for symmetry-lowering in-plane bond relaxations we adopted a (2 × 1) basal interface cell (5.489 Å × 3.169 Å) for all calculations. The supercell dimension normal to the interface for all our calculations was 38 Å. For each separated or bonded configuration the atomic coordinates were fully relaxed to their zero force positions. A 7 × 4 × 1 Monkhorst−Pack k point grid was used in all calculations together with a 400 eV plane wave cutoff to achieve a force accuracy of 0.01 eV/Å. For a slab of cross-sectional area $A = 17.39$ Å^2 we use the relation $E_{total} = E_{bulk}{}^{\alpha} + E_{bulk}{}^{\beta} + A(\Gamma + \sigma^{\alpha} + \sigma^{\beta})$, where σ^{α} and σ^{β} are the average free surface energies of the separated slabs. The converged total slab energies and surface energies for each model were then combined to yield the interface energy: $\Gamma_m(\mu_C, \mu_{Zr}) = [E_{total} - (E_{bulk}{}^{\alpha} + E_{bulk}{}^{\beta}) - A(\sigma^{\alpha} + \sigma^{\beta})]/A$. The surface energies σ^{ZrB_2} and σ^{SiC} were calculated separately using a seven-layer slab procedure following Yamamoto et al.[20] The results are listed in Table 1, which shows that Zr-terminated interfaces are the most stable. We find that the only thermodynamically stable configuration (model A) involves a distorted tetrahedral silicon center bonded to one C ($b_{SiC} = 1.89$ Å) and three Zr atoms ($b_{SiZr} = 2.82$ Å). The Zr−Si bond distance is similar to the 2.9 Å found in bulk $ZrSi_2$. The next most favorable (least metastable) configuration has one silicon atom bonded to one boron and three carbons, as shown in model B. The remaining two models also contain reasonable coordinations of tetrahedral carbon (models C and D) bonded to the zirconium layer of ZrB_2 (we find that GGA predicts bond lengths 1−2% larger than those observed).

The epitaxial growth of SiC on ZrB_2 should be characteristic of joining two dissimilar materials with low-compressibility, highly rigid structures. If the interface bonding is weaker than that of bulk SiC or ZrB_2 then the epitaxy may occur via bond deformation (or defect formation), which in this case is localized to a single interface layer. Figure 8a shows the metrology of the SiC(111)−ZrB_2(0001) interface based on phase-contrast XTEM imaging. Note the remarkable planarity and bulklike character of the SiC and ZrB_2 lattice immediately adjacent to the interface layer, indicating that the misfit is confined within this plane of atoms. A comparison of the experimental micrograph (Figure 8a) with detailed HRTEM simulations using the microscope parameters and the optimized first principles interface atomic positions (Figure 8b) shows that the horizontal bright rows spots in the top half of the images

(19) Kresse, G.; Furthmuller, J. *Phys. Rev. B* **1996**, *54*, 11169. Kresse, G.; Furthmuller, J. *Comput. Mater. Sci.* **1996**, *6*, 15. A discussion of the ultra-soft pseudopotentials used in the VASP code is given in Kresse, G.; Hafner, J. *J. Phys.: Condens. Matter* **1994**, *6*, 8245.
(20) Yamamoto, K.; Kobayashi, K.; Kawanowa, H.; Souda, R. *Phys. Rev. B* **1999**, *60*, 15617.
(21) Vajeeston, P.; Ravindran, P.; Ravi1, C.; Asokamani, R. *Phys. Rev. B* **2001**, *63*, 45115.
(22) Grossner, U.; Furthmüller, J.; Bechstedt, F. *Phys. Rev. B* **2001**, *46*, 165308.
(23) Boettger, J. C. *Phys. Rev. B* **1994**, *49*, 16798.

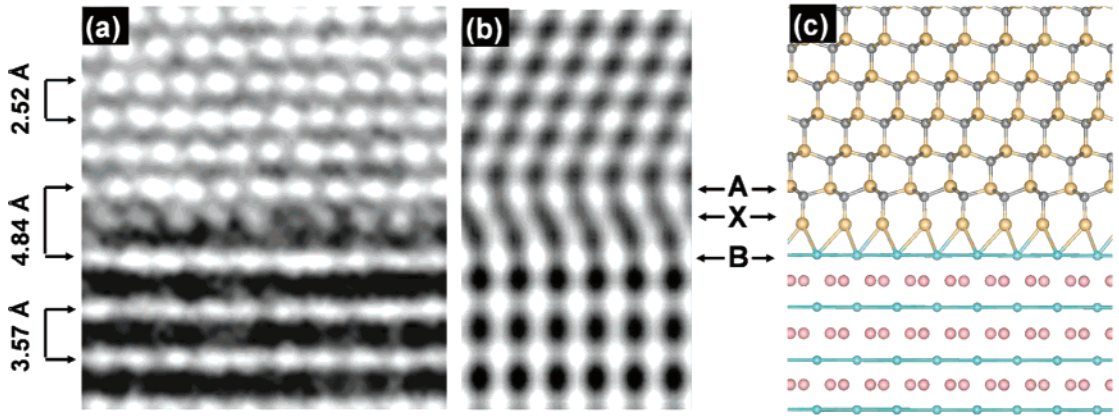

Figure 8. Comparison of the observed (a) and simulated (b) XTEM micrographs of the SiC−ZrB_2 interface microstructure. The simulated XTEM pattern (b) was obtained from the ab initio interface structure corresponding to the lowest energy model A, shown in Figure 7. This comparison suggests that the transition layer (X), above, consists of silicon atoms bonded to adjacent Zr and C atomic rows as shown in model structure c. Yellow, black, blue and pink spheres represent the atoms Si, C, Zr and B, respectively.

are Si−C (111) double layers while the bright rows in the bottom half correspond to zirconium basal planes. Note the excellent agreement between the experimental and simulated patterns (Figure 8a,b, respectively). The interlayer spacings in pure SiC (2.52 Å) and ZrB_2 (3.57 Å) were determined by electron microscopy and subsequently used to infer the interface distances from simple scaling of the known SiC and ZrB_2 interlayer values. As shown in Figure 8 the initial bulklike SiC layer (A) and the terminating bulklike ZrB_2 layer (B) are separated by 4.84 Å and ensconce a transition interface layer (X). This layer is separated from the SiC row by 2.09 Å which is significantly less than the bulk Si−C interlayer spacing of 2.52 Å. On the other hand, layer X is separated from the ZrB_2 layer by 2.75 Å, which again is significantly less than the Zr−Zr interplanar spacing of 3.57 Å. Our simulations clearly show that layer X cannot be pure Zr. From our ab initio interface energy calculations we have determined that the most stable interface structure (model A, Figure 7) contains Si−Zr bonds which are expected to be weaker than either Si−C (layer A) or Zr−Zr (layer B) bonds. Because the weaker Si−Zr bonds are more likely to deform, this bonding arrangement may provide a mechanism for mismatch accommodation between the two materials. The interlayer distances at the interface are quantitatively consistent with lowest energy interface model (A). It should be noted that in our simulation studies a slight strain of $\sim 3.2\%$ was imposed on the SiC lattice to commensurate with the ZrB_2 lattice. This was done to make the calculations tractable. Our experimental data show, however, that the SiC layer is completely relaxed. Small differences in the lateral registry between our simulated interface and that observed are due to this "coherent lattice" approximation.

Conclusion

Low-temperature pathways and novel heteroepitaxy concepts have been developed and then used to achieve integration of germanium and silicon carbide films and islands with Si(111) substrates. A zirconium diboride epitaxial layer has been used as the template to obtain commensurate growth in both cases despite the large lattice mismatches between the hexagonal template and the cubic films. For Ge(111)/ZrB_2(0001) heterostructures of islands the large lattice discrepancy between the two materials is accommodated with pure edge dislocations as a result of a commensurate match of five lattice rows of ZrB_2 aligning with four lattice rows of Ge. The ratio of the in-plane lattice dimensions, d_{Ge-Ge}/a_{ZrB_2}, is 5/4, allowing the exact alignment of four lattice rows of Ge with five rows of ZrB_2 leading to the formation of a perfectly commensurate interface. Strain-free SiC films and nanoscale islands, devoid of stacking faults, grow epitaxially on zirconium diboride at 800 and 900 °C, respectively. A perfect and atomically abrupt interface is observed between the highly planar ZrB_2 surface and the β-SiC film within the first monolayer of growth.

Acknowledgment. The work was supported by NSF DMR-0221993 and ARO W911NF-04-1-0256.

CM0510918